catalysts

MDPI

Article

Enhanced Performance of Supported Ternary Metal Catalysts for the Oxidation of Toluene in the Presence of Trichloroethylene

Tiantian Dong [1], Kun Liu [2], Ruyi Gao [1], Hualian Chen [1], Xiaohui Yu [1], Zhiquan Hou [1], Lin Jing [1], Jiguang Deng [1], Yuxi Liu [1,*] and Hongxing Dai [1,*]

[1] Beijing Key Laboratory for Green Catalysis and Separation, Key Laboratory of Beijing on Regional Air Pollution Control, Key Laboratory of Advanced Functional Materials, Education Ministry of China, Department of Environmental Chemical Engineering, Faculty of Environment and Life, Beijing University of Technology, Beijing 100124, China; ttdbjut@163.com (T.D.); gaoruyi@emails.bjut.edu.cn (R.G.); chenhl@emails.bjut.edu.cn (H.C.); 18697203595@163.com (X.Y.); u11052126@163.com (Z.H.); jinglin@bjut.edu.cn (L.J.); jgdeng@bjut.edu.cn (J.D.)

[2] Institute of Optical Functional Materials for Biomedical Imaging, School of Chemistry and Pharmaceutical Engineering, Shandong First Medical University & Shandong Academy of Medical Sciences, Taian 271016, China; liukun2436@126.com

* Correspondence: yxliu@bjut.edu.cn (Y.L.); hxdai@bjut.edu.cn (H.D.); Tel.: +86-10-6739-6118 (Y.L. & H.D.)

Abstract: Chlorinated volatile organic compounds (CVOCs), even in small quantities, can cause Pt-based catalyst poisoning. Improving the low-temperature chlorine resistance of catalysts is of vital importance for industrial application, although it remains challenging. Considering actual industrial production, a TiO_2-supported ternary metal catalyst was prepared in this work to study the catalytic oxidation of multicomponent VOCs (toluene and trichloroethylene (TCE)). Among all of the samples, $PtWRu/TiO_2$ and $PtWCr/TiO_2$ exhibited the best catalytic performance for toluene oxidation. In the mixed VOC oxidation, the $PtWCr/TiO_2$ sample showed the best catalytic activity for toluene combustion (a toluene conversion of 90% was achieved at 258 °C and a space velocity of 40,000 mL g^{-1} h^{-1}, and the specific reaction rate and turnover frequency at 215 °C were 44.9 × 10^{-6} mol $g_{Pt}{}^{-1}$ s^{-1} and 26.2 × 10^{-5} s^{-1}). The $PtWRu/TiO_2$ sample showed the best catalytic activity for TCE combustion (a TCE conversion of 90% was achieved at 305 °C and a space velocity of 40,000 mL g^{-1} h^{-1}, and the specific reaction rate and turnover frequency at 270 °C were 9.0 × 10^{-6} mol $g_{Pt}{}^{-1}$ s^{-1} and 7.3 × 10^{-5} s^{-1}). We concluded that the ternary metal catalysts could greatly improve chlorine desorption by increasing the active lattice oxygen mobility and surface acidity, thus reducing chlorinated byproducts and other serious environmental pollutants. This work may serve as a reasonable design reference for solving more practical industrial production emissions of multicomponent VOCs.

Keywords: supported ternary metal catalysts; Pt-based catalysts; volatile organic compounds; toluene and TCE combustion; chlorine-resistant ability

Citation: Dong, T.; Liu, K.; Gao, R.; Chen, H.; Yu, X.; Hou, Z.; Jing, L.; Deng, J.; Liu, Y.; Dai, H. Enhanced Performance of Supported Ternary Metal Catalysts for the Oxidation of Toluene in the Presence of Trichloroethylene. *Catalysts* **2022**, *12*, 541. https://doi.org/10.3390/catal12050541

Academic Editors: Yu Huang and Qian Zhang

Received: 4 April 2022
Accepted: 13 May 2022
Published: 16 May 2022

1. Introduction

Volatile organic compounds (VOCs) are harmful to the human body even at very low concentrations (ppm level) [1]. VOCs can also cause significant impacts on the surrounding environment through ozone, secondary aerosol, and photochemical smog generation [2–4]. Studies have shown that industrial VOC emissions are often complex, containing a variety of components [5]. Among these, chlorinated volatile organic compounds (CVOCs) are extremely toxic and exhibit strong chemical stability, are considered harmful gas pollutants, and are listed as highly harmful emissions in most countries [6,7].

Supported precious metals such as Pt, Pd, and Ru exhibit high efficiency in the catalytic combustion of VOCs at relatively low temperatures [8,9]. Reports have shown that doping the second metal or even third metal to precious metals will achieve a synergistic

effect by changing the electronic or geometric structure of the precious metal catalyst. For example, Hosseini et al. [10] investigated the catalytic combustion of toluene over a sequence of bimetallic catalysts and found that the catalytic activity of the Au-Pd catalysts was superior to single-metal Au and Pd catalysts. In addition, Zheng's group [11] prepared a Pt–Fe–Ni ternary metal alloy and found that there was an interface composed of Fe^{3+}–OH–Pt on the catalyst, which was beneficial to the adsorption and oxidation of CO. Priya et al. [12] prepared Pt–Sn–Ce/MC ternary metal catalysts (MC is mesoporous carbon) by the method of impregnation reduction. The Pt–Sn–Ce/MC catalysts showed superior activity than the obtained Pt–Sn/MC and Pt–Ce/MC for ethanol oxidation. The better performance of mesoporous-carbon-supported ternary metal catalysts is attributed to the significant increase in electrochemical active surface area and the smaller particle size of NPs. Yang et al. [13] reported that a Co_3O_4-supported $Ag_{0.75}Au_{1.14}Pd$ catalyst with higher adsorbed oxygen concentration and good low-temperature reducibility showed excellent catalytic activity for methanol oxidation. Barakat et al. [14] studied the synergistic effect of Pd-Nb-V/TiO_2 for toluene oxidation, revealing that the doping of Nb and V enhanced the catalytic activity, and temperature-programmed reduction work indicated that the link of Pd with V allowed for easy catalyst reduction. This was attributed to the modified redox properties of the samples.

Pt-based catalysts with exceptional redox performance and high ability to activate C-O and C-H have been used commercially for the catalytic elimination of VOCs, such as benzene and toluene [15]. However, these catalysts will be severely inactivated or even poisoned by trace CVOCs [16]. In addition, high prices are an uncontrollable factor. Previously, our research team [17] reported an effective method to add inexpensive auxiliaries such as transition metals to modify precious metals and form bimetallic catalysts. Currently, only studies on the catalytic combustion of CVOCs have been reported in the relevant literature. Zhang et al. [6] and Dai et al. [18] found that Ru-based materials were excellent catalysts for detaching CVOCs, due to their strong ability to crack C-Cl bonds and decrease Cl deposition. Zhang et al. [19] also examined the active ingredients (Ru and Cr) incorporated into CVOC combustion, which were useful for the production and desorption of Cl_2. Ru and Cr loading has been widely used to advance deacon reactions in support of Cl_2 production. In dichloromethane (DCM) oxidation, Weng et al. [20] determined good catalytic activity as a result of the presence of rich Mn (IV) species. Hence, the development of a good catalyst suitable for the elimination of multicomponent VOCs is critical in future work.

In this work, PtW*M* (*M* = Ru, Cr, Mn) ternary metal nanocrystals were prepared using the solvothermal method and loaded onto a TiO_2 carrier. Subsequently, the PtWMO_x/TiO_2 catalyst was obtained after calcination, and the effect of trichloroethylene (TCE) as a co-pollutant on the catalytic performance of the supported platinum-based ternary metal catalysts for toluene oxidation was studied in detail. The supported ternary metal catalysts showed better low-temperature catalytic activity and good chlorine resistance performance compared to the supported Pt counterpart. To the best of our knowledge, there have been no studies reported in the literature on the effects of Pt-based ternary metal catalysts for the simultaneous catalytic purification of VOCs and CVOCs.

2. Results and Discussion

2.1. Catalytic Performance

Single-ingredient and mixed experiments were conducted for several samples at a fixed flow. First, the catalytic activities of the as-obtained catalysts were tested according to the oxidation of toluene. Over the Pt/TiO_2 catalyst, the temperature needed for 90% conversion of toluene ($T_{90\%}$) was 178 °C. With W doping, the $T_{90\%}$ for toluene decreased to 162 °C. For the ternary PtW*M*/TiO_2 (*M* = Ru, Cr, Mn) catalysts, the $T_{90\%}$ for toluene was about 160 °C. These results showed a slight improvement compared to Pt/TiO_2 and PtW/TiO_2. As shown in Figure 1A, these results suggested that the inclusion of *M* (*M* = Ru, Mn, Cr) made it easier to crack C–H and C–C. In addition, we added 200 ppm of TCE at the temperature when toluene was almost completely transformed, to observe

the effects on toluene catalytic performance, and the results are shown in Figure 1B. When TCE was added to the reaction system for 30 min, the conversion of toluene on Pt/TiO_2 and PtW/TiO_2 decreased to 20% and 24%, respectively. When TCE was added for 24 h, the conversion of toluene on Pt/TiO_2 and PtW/TiO_2 catalysts stabilized at 15% and 20%, respectively. $PtWRu/TiO_2$, $PtWCr/TiO_2$ and $PtWMn/TiO_2$ decreased to about 45.0%, 50.0%, and 45.0%, respectively, and each catalyst could be kept for 24 h. However, in the absence of TCE, toluene conversion could not restore over Pt/TiO_2 and PtW/TiO_2 catalysts within 12 h, while toluene conversion on $PtWRu/TiO_2$ and $PtWCr/TiO_2$ immediately recovered to the initial value at this temperature within the first 30 min of TCE be cut off, and the toluene conversion over $PtWMn/TiO_2$ successfully recovered after 2 h. This phenomenon indicated that $PtWM/TiO_2$ was more chlorine-resistant than Pt/TiO_2 or PtW/TiO_2. The introduction of the third metal increased the removal of Cl species.

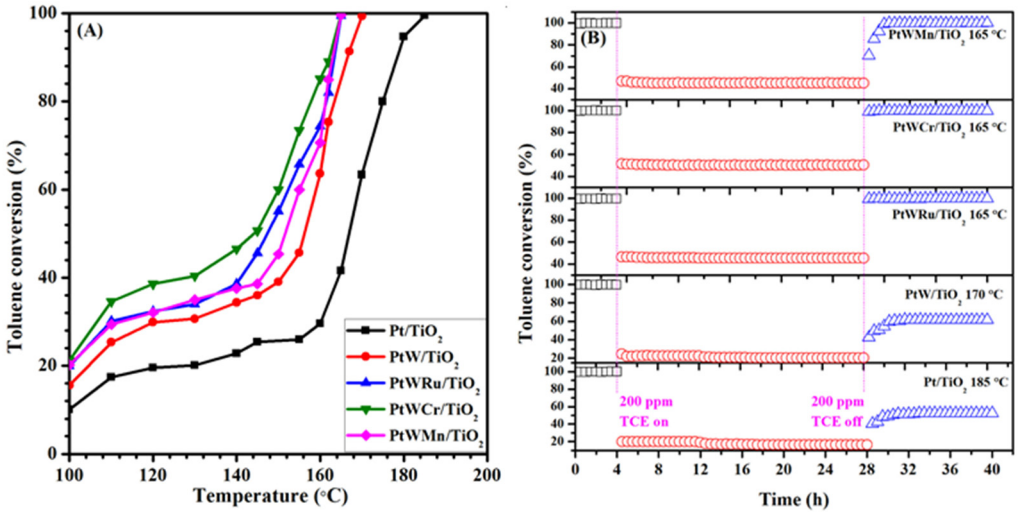

Figure 1. (**A**) Toluene conversion as a function of the reaction temperature and (**B**) effect of TCE on the catalytic activity of the as-obtained catalysts for toluene oxidation at SV = 40,000 mL/(g h).

We also fabricated 1000 ppm toluene, 200 ppm TCE, and 20% oxygen into a mixed gas, which carried out the catalytic oxidation of the mixed VOCs, under the same conditions as the single component experiment (shown in Figure 2A,B). For the Pt/TiO_2 and PtW/TiO_2 catalysts, the reaction temperature of toluene increased when mixed with TCE, followed by a conversion curve shift to higher temperatures. For Pt/TiO_2, the negative influence was very strong when $T_{50\%}$ and $T_{90\%}$ increased by 96 °C and 132 °C after mixing with TCE, respectively. The results of PtW/TiO_2 and Pt/TiO_2 showed similar trends. The catalytic activity of ternary metal catalyst $PtWM/TiO_2$ significantly improved, and $T_{50\%}$ and $T_{90\%}$ decreased by 34–44 °C and 41–55 °C compared to Pt/TiO_2 and PtW/TiO_2. In addition, the $T_{90\%}$ of the ternary metal catalyst during TCE oxidation reached the maximum decrease range of about 60 °C compared to PtW/TiO_2, while Pt/TiO_2 still failed to reach $T_{90\%}$, even at 500 °C. For the WM/TiO_2 catalysts, the conversion of both toluene and TCE was less than 20% before 300 °C, indicating that without Pt species, the catalytic performance of the bimetallic samples was greatly limited. The reaction rate and turnover frequencies (TOFs) at 215 °C (toluene) and 270 °C (TCE) were calculated and are listed in Table 1 to evaluate the internal activity of the obtained catalyst. $PtWCr/TiO_2$ appeared to have a higher reaction rate and TOF_{Pt} (for toluene oxidation, 44.9 umol/(g_{Pt} s) of 26.2 ($\times 10^{-5}$ s^{-1})), while $PtWRu/TiO_2$ had a higher TCE oxidation rate of 9.0 umol/(g_{Pt} s) and TOF_{Pt} of 7.3 ($\times 10^{-5}$ s^{-1}). These results suggested that the ternary metal catalyst could better tolerate Cl influence compared to Pt/TiO_2 and PtW/TiO_2. This was attributed to the fact that the catalysts could easily desorb Cl species, which will be explained by subsequent characterization. Comparisons of toluene oxidation activity for toluene alone

and mixed VOCs are shown in Figure S4 and Table S1 (note: all were mixed VOCs as the research object).

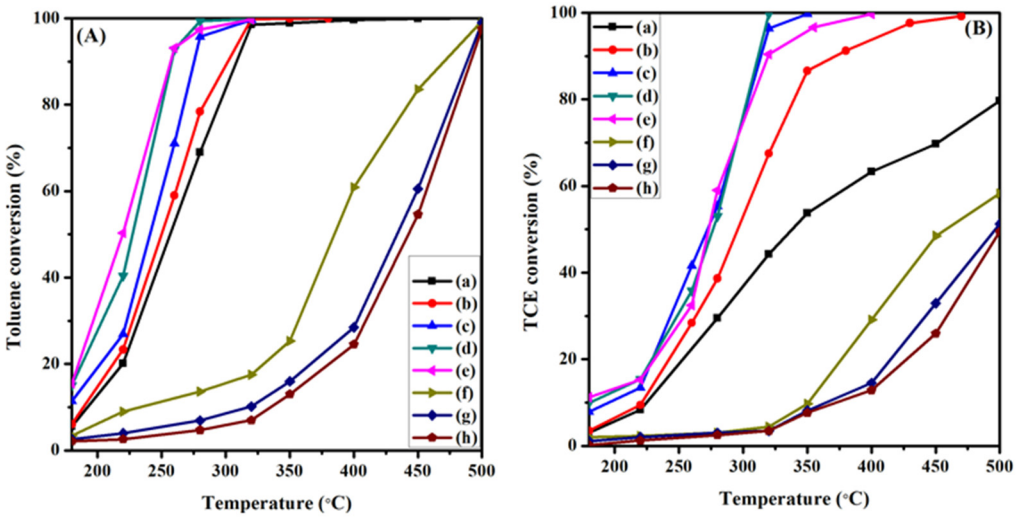

Figure 2. (**A**) Toluene and (**B**) TCE conversion (in mixture) as a function of temperature over (a) Pt/TiO_2, (b) PtW/TiO_2, (c) $PtWRu/TiO_2$, (d) $PtWCr/TiO_2$, (e) $PtWMn/TiO_2$, (f) WRu/TiO_2, (g) WCr/TiO_2, and (h) WMn/TiO_2 and SV = 40,000 mL/(g h).

Table 1. Catalytic activity, specific reaction rates, and TOFs (toluene oxidation at 215 °C, TCE oxidation at 270 °C) of the as-obtained samples for mixed VOC oxidation.

Sample	Toluene Conversion		TCE Conversion		Specific Reaction Rates ($\times 10^{-6}$ mol/(g_{Pt} s))		TOF_{Pt} ($\times 10^{-5}$ s^{-1})		Metal Dispersion (%)
	$T_{50\%}$ (°C)	$T_{90\%}$ (°C)	$T_{50\%}$ (°C)	$T_{90\%}$ (°C)	Toluene	TCE	Toluene	TCE	
Pt/TiO_2	260	310	340	>500	17.3	4.9	9.4	2.6	36
PtW/TiO_2	250	296	300	378	20.5	6.3	13.3	4.1	30
$PtWRu/TiO_2$	240	275	272	305	25.0	9.0	20.3	7.3	24
$PtWCr/TiO_2$	225	258	276	300	44.9	8.4	26.2	6.1	27
$PtWMn/TiO_2$	216	255	272	318	36.2	8.0	25.7	5.1	34

2.2. Crystal Structure, Morphology, and Surface Area

Figure 3 shows the XRD patterns of the as-obtained fresh and used samples (before and after reaction). According to the XRD patterns (JCPDS PDF# 76-1939) for standard titanium dioxide with a rutile crystal structure, no clear diffraction peaks of Pt or W/Ru/Cr/Mn species were detected in the XRD patterns of the supported catalysts. This was possibly due to the decreased loading and good dispersion of the noble metal NPs on the support surface. In addition, the used catalysts after 40 h reaction had no obvious crystal change compared with the fresh catalysts. The morphologies of the metal NPs were measured by TEM, and their average particle diameters were acquired by data analysis, as displayed in Figure S1 and Table 1. In addition, Figure 4 shows the TEM images, HAADF-STEM images, elemental maps of the as-obtained samples, and EDX line scan images of $PtWMn/TiO_2$. The HADDF-STEM images and EDX elemental mappings of the obtained samples showed that Pt, W, and *M* were highly distributed on the catalyst surface. We also obtained line scanning data of the $PtWMn/TiO_2$ catalyst, which showed that a ternary metal catalyst was successfully prepared. The TEM images of Pt/TiO_2 and PtW/TiO_2 are shown in Figure S2, and the BET statistics are provided in Table 2 and Figure S3.

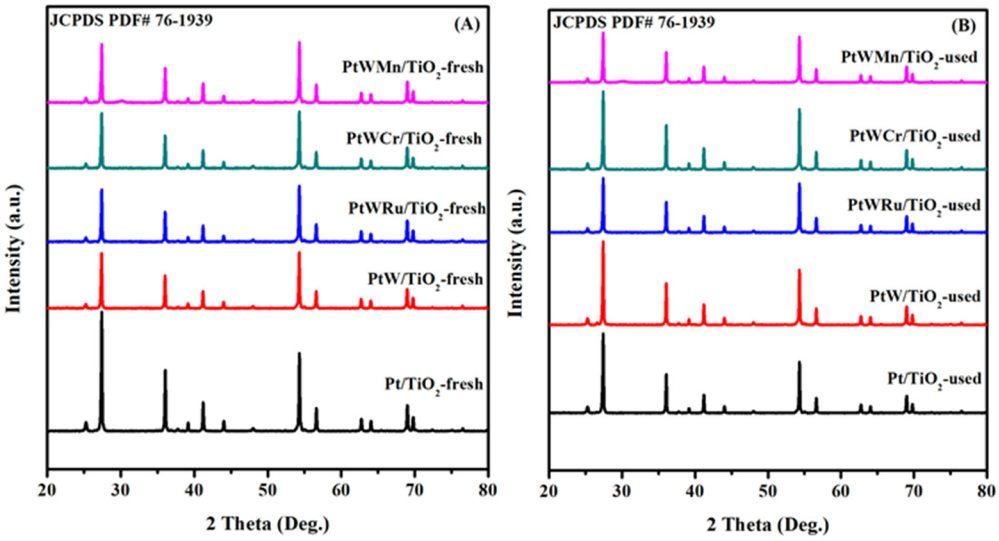

Figure 3. XRD patterns of the as-obtained samples: (**A**) fresh catalysts and (**B**) used catalysts.

Table 2. Average particle sizes, actual metal loadings, BET surface areas, and surface elemental compositions of the as-obtained samples.

Sample	Particle Size [a] (nm)	Actual Pt Loading [b] (wt%)	Actual W Loading [b] (wt%)	Actual Ru Loading [b] (wt%)	Actual Cr Loading [b] (wt%)	Actual Mn Loading [b] (wt%)	BET Surface Area (m^2/g)	Surface Elemental Composition [c] (mol/mol)					
								Pt^0/Pt^{2+} [c]	O_{latt}/O_{ads}	W^{6+}/W^{5+}	Ru^{4+}/Ru^0	Cr^{6+}/Cr^{3+}	$Mn^{4+}/Mn^{3+}/Mn^{2+}$
Pt/TiO_2	3.0	0.43					8.2	2.1	4.3				
PtW/TiO_2	9.1	0.45	4.86				9.1	1.8	4.9	1.9			
$PtWRu/TiO_2$	6.2	0.42	4.85	1.89			7.7	1.5	5.5	3.1	0.4		
$PtWCr/TiO_2$	7.3	0.45	4.90		0.96		13.2	1.5	5.1	10.3		0.6	
$PtWMn/TiO_2$	8.2	0.43	4.88			0.94	12.0	5.1	4.5	9.5			1.4:1.5:1

[a] Calculated according to the HAADF-STEM images; [b] determined by ICP-AES; [c] determined by XPS.

2.3. Redox Ability and Oxygen Mobility

H_2 temperature-programmed reduction (H_2-TPR) (Figure 5A) experiments were carried out to determine the reducibility of the as-obtained samples. A smaller peak was observed over $PtWRu/TiO_2$ at 160–200 °C, which was attributed to the reduction of RuO_x species [21,22]. In addition, the Pt/TiO_2, PtW/TiO_2, $PtWRu/TiO_2$, $PtWCr/TiO_2$, and $PtWMn/TiO_2$ catalysts had peaks at 400 °C, 384 °C, 375 °C, 423 °C, and 395 °C respectively, which were attributed to the reduction of the surface Ti^{4+} to Ti^{3+} through the spillover of H atoms chemically adsorbed on the reduced Pt [23,24]. The peaks at 562 °C for PtW/TiO_2, at 564 °C for $PtWRu/TiO_2$, at 564 °C for $PtWCr/TiO_2$, and at 560 °C for $PtWMn/TiO_2$ were attributed to the reduction of surface coordination unsaturated W^{6+} species. The catalyst with Ru doping adsorbed a large amount of H_2 overflow, which accelerated the reduction of WO_x and TiO_2. This indicated strengthened interactions between the metal and support [25]. All of the above samples had peaks at 696 °C, 777 °C, 733 °C, 789 °C, and 789 °C, respectively, indicating the reduction of W^{5+} to W^0, as well as Ti^{4+} in the bulk phase to Ti^{3+} [26].

To determine the oxygen species mobility of the as-obtained samples, the O_2 temperature program desorption (O_2-TPD) experiment was performed, and the results are shown in Figure 5B. The peaks could be divided into two areas, one of which was 100–300 °C, while the other was 300–600 °C. The peaks below 300 °C were attributed to the desorption of surface adsorption oxygen species, while the peaks between 300 and 600 °C were attributed to the desorption of surface lattice oxygen species, and the desorption peak above 600 °C was attributed to the more stable bulk lattice oxygen [27]. In particular, the peak areas of surface lattice oxygen species noticeably increased over the ternary metal catalysts. These results showed that the doping of transition metals (Ru, Cr, and Mn) to PtW/TiO_2 clearly increased the lattice oxygen migration of the samples, indicating that $PtWM/TiO_2$ possessed a better redox cycle in CVOC oxidation.

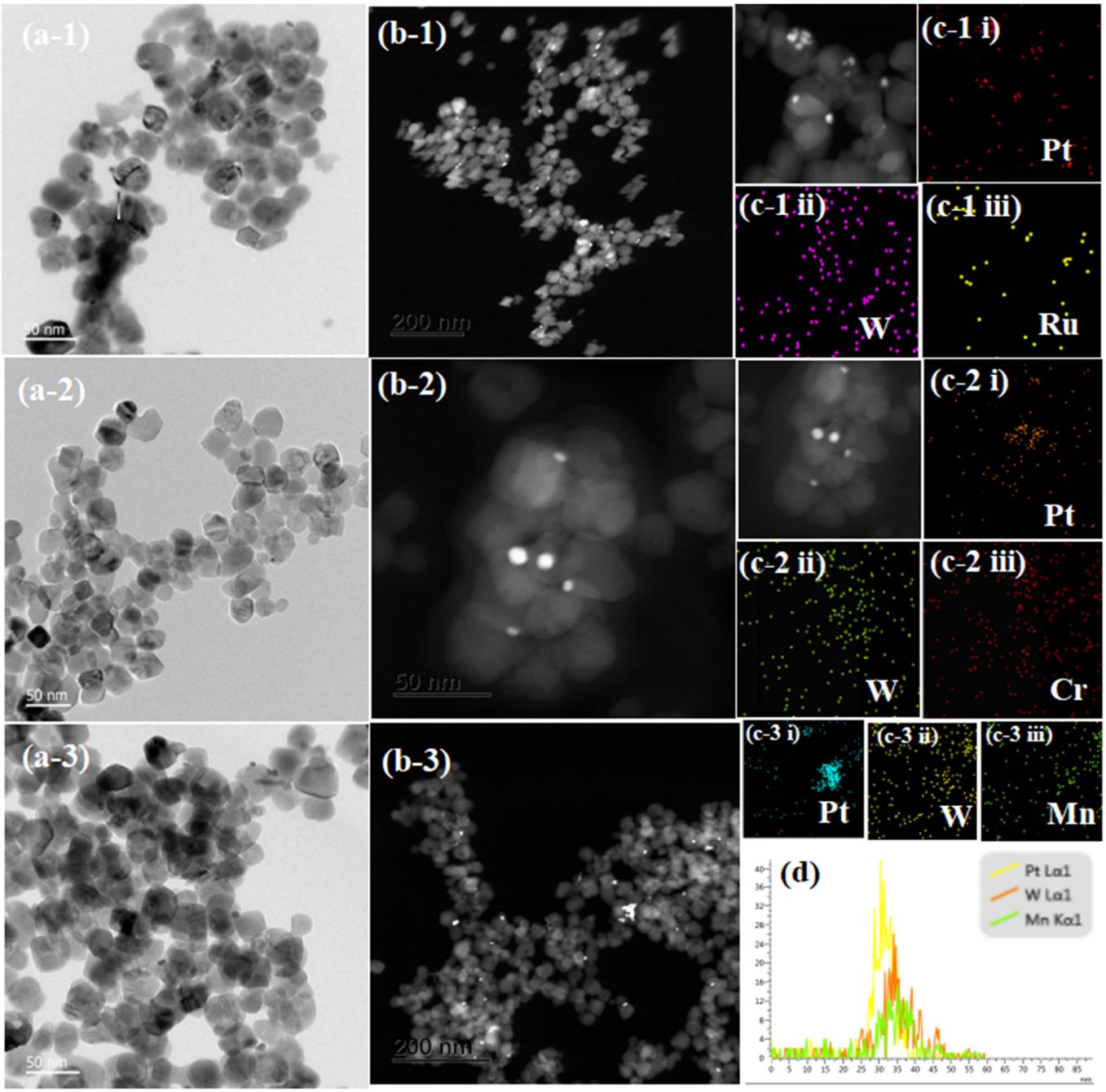

Figure 4. (**a-1**–**a-3**) TEM images, (**b-1**–**b-3**) HAADF-STEM images, and (**c-1**–**c-3**) EDX elemental mappings of the PtWRu/TiO_2, PtWCr/TiO_2, and PtWMn/TiO_2 samples; (**d**) EDX line scan images of PtWMn/TiO_2.

2.4. Surface Elemental Composition

The surface elemental composition of the as-obtained samples was tested by XPS (Figure 6). The O 1s XPS spectra (Figure 6A) with an asymmetric peak could be divided into three components. The signal peak at 529.8 eV corresponded to the characteristic peak of the lattice oxygen (O_{latt}) on the catalyst surface, while the signal peak at 531.4 eV was the characteristic peak of adsorbed oxygen (O_{ads}, such as O_2^-, O_2^{2-}, or O^-) on the catalyst surface, and the signal peak at 533.0 eV was the characteristic peak of molecular water [28]. Figure 6B shows the Ru 3p spectrum, where the peaks at 458.8 eV and 461.1 eV were Ru^0 species, and the peak at 464.3 eV was Ru^{4+} species [29,30]. Figure 6C shows the spectrum of Cr 2p, where the asymmetric peak was divided into binding energies of

577.0 eV, 579.1 eV, 586.8 eV, and 589.4 eV, the components of 577.0 eV and 586.8 eV belonged to Cr^{3+} species, and the components at 579.1 eV and 589.4 eV were assigned to the signal of Cr^{6+} species [31]. Figure 6D presents the spectrum of Mn 2p, showing that the peak could be divided into three signal peaks at 640.2, 641.6, and 644.6 eV. The signal peak at 640.2 eV was the characteristic peak of surface Mn^{2+} species, the signal peak at 641.6 eV was the characteristic peak of surface Mn^{3+} species, and the signal peak at 644.6 eV was the characteristic peak of surface Mn^{4+} species. The coordination of Mn ions with different valence states contributed to their excellent redox ability [32,33]. The spectra of Pt 4f, Ti 2p, and W 4f are shown in Figure S5.

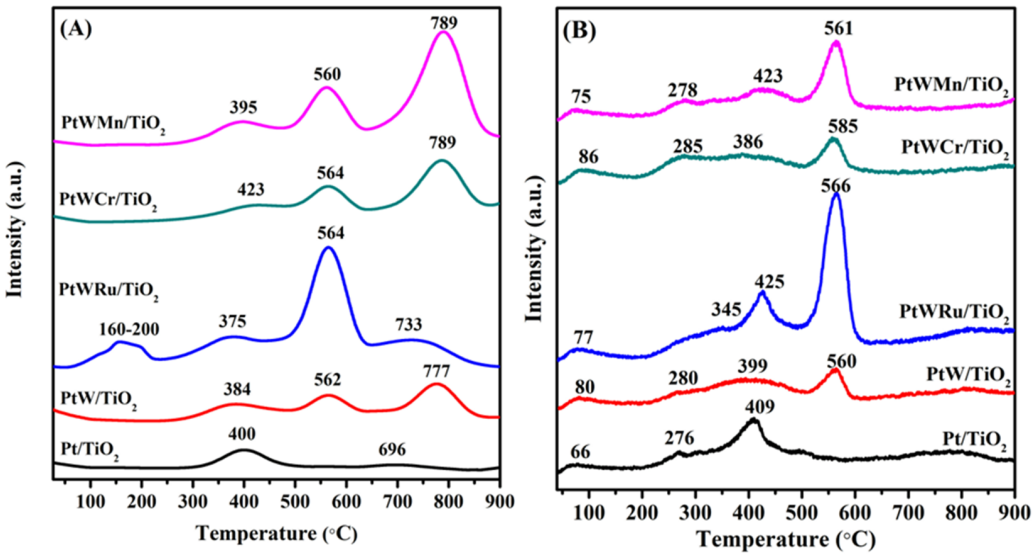

Figure 5. (**A**) H_2-TPR profiles of the as-obtained samples and (**B**) O_2-TPD profiles of the as-obtained samples.

2.5. NH_3-TPD, Toluene&TCE-TPD, and Toluene&TCE-TPSR

The acid–base properties of catalysts are key parameters that affect catalytic activity and selectivity, especially for CVOC oxidation. In this work, NH_3 temperature-programmed desorption (NH_3-TPD) experiments were carried out to measure the surface acidity of the samples. Figure 7 shows that the samples' peak at 270–400 °C corresponded to the desorption of NH_3 at the medium acid site, while the peak at 400–600 °C corresponded to the desorption of NH_3 at the strong acid site. Pt/TiO_2 had one strong acid site desorption peak, and the bimetal and ternary metal samples had two strong acid site desorption peaks. We clearly observed that the desorption amount of NH_3 over the bimetal metal samples was much larger than that over Pt/TiO_2, indicating that the addition of WO_x increased the acidity of the samples. According to previous reports, the weak and strong acid sites were mainly caused by Lewis [34] and Brønsted acids [35], respectively. As can be seen from Figure 7, MO_x/TiO_2 further provided both Brønsted acid sites (*M*–OH) and Lewis acid sites (M^{n+} and Ti^{3+}/Ti^{4+}). In addition, steady Brønsted acidity is beneficial for CVOC oxidation, as it can continuously adsorb CVOCs and supply protons. Lewis acidity can also be very useful for the activation of the C–Cl bond from CVOCs [36]. In this work, the Lewis acidity was due to W^{6+}/W^{5+} that forms between WO_x and the carrier [37,38].

The mixed toluene and TCE temperature-programmed desorption (VOCs-TPD) test was conducted to assess the adsorption and oxidizing ability of the multiple VOCs over the obtained catalysts. As shown in Figure 8A, the peaks of each sample were between 50 °C and 80 °C, and these belonged to toluene species with weak chemical adsorption on the samples. The adsorption capacity of toluene on PtW/TiO_2 was slightly higher than over Pt/TiO_2, indicating that the doping of W enhanced the chemisorption capacity of toluene over the sample. After further alloying of Ru/Cr/Mn, the adsorption capacity of toluene over the samples increased significantly. Figure 8B shows the desorption peak of the TCE species over the samples, and weak signals of the TCE species were detected

over PtWRu/TiO_2, PtWCr/TiO_2, and PtWMn/TiO_2. However, the TCE species were not detected over Pt/TiO_2 and PtW/TiO_2, indicating that the TCE adsorption capacity over the two samples is relatively low. Another characteristic of the fragment was CO_2 (Figure 8C). The peak at 50–250 °C was attributed to the reaction of surface electrophilic oxygen species with adsorbed VOCs, and the peak at 300–800 °C was the reaction of active lattice oxygen species with strongly adsorbed VOCs. In addition, PtWRu/TiO_2 and PtWMn/TiO_2 showed good performance for the deep oxidation of the mixed VOCs in the high-temperature region (300–600 °C), indicating that these catalysts contained more abundant active lattice oxygen species, which was consistent with the O_2-TPD results. According to related literature reports [20], during oxidation of CVOCs on the catalyst, due to the two active centers, one acidic site adsorbed chlorine, while the other basic site adsorbed carbon, and the further redox sites generated CO_2 and H_2O. These results showed that the addition of the third metal formed an adsorption center through M^{n+}–O, which was also a redox site.

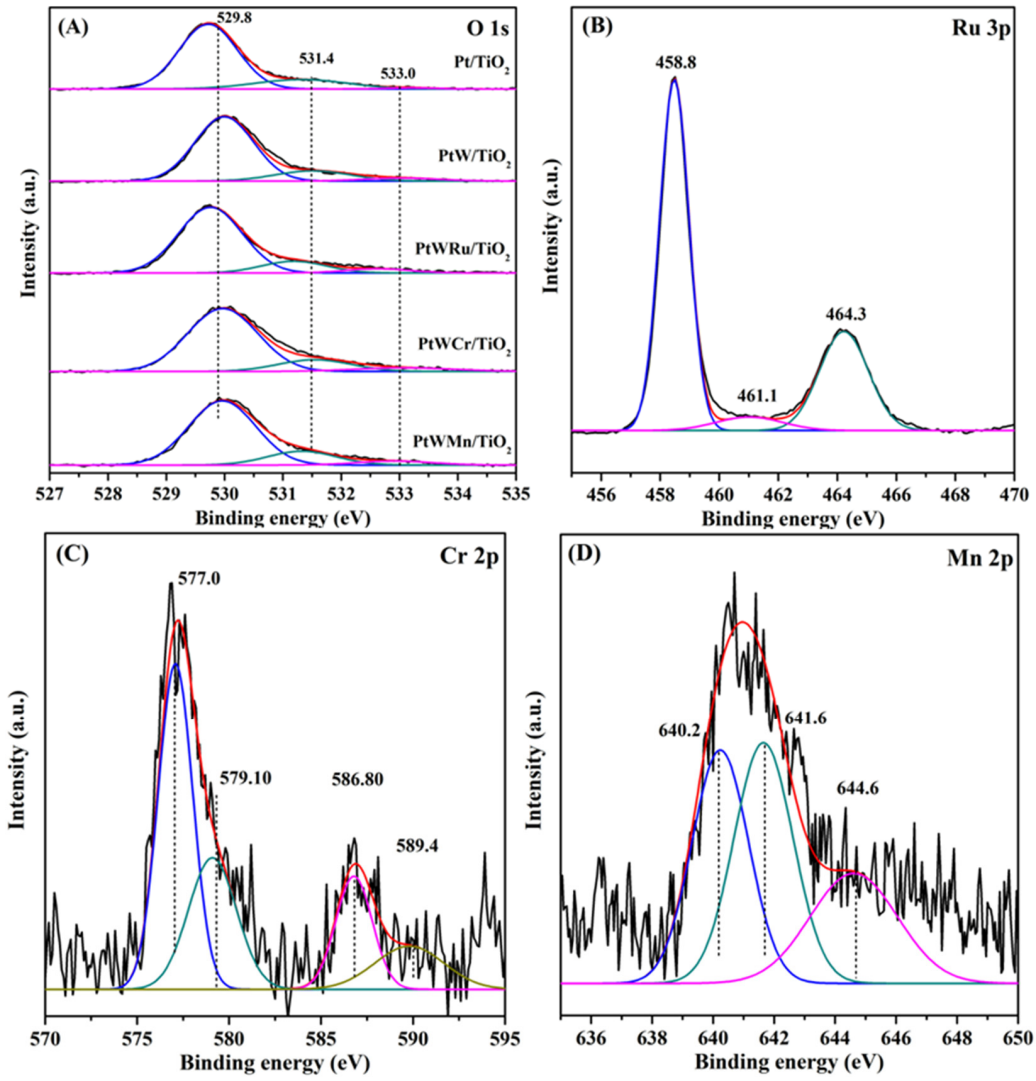

Figure 6. XPS spectra of (**A**) O 1s, (**B**) Ru 3p, (**C**) Cr 2p, and (**D**) Mn 2p in each of the samples.

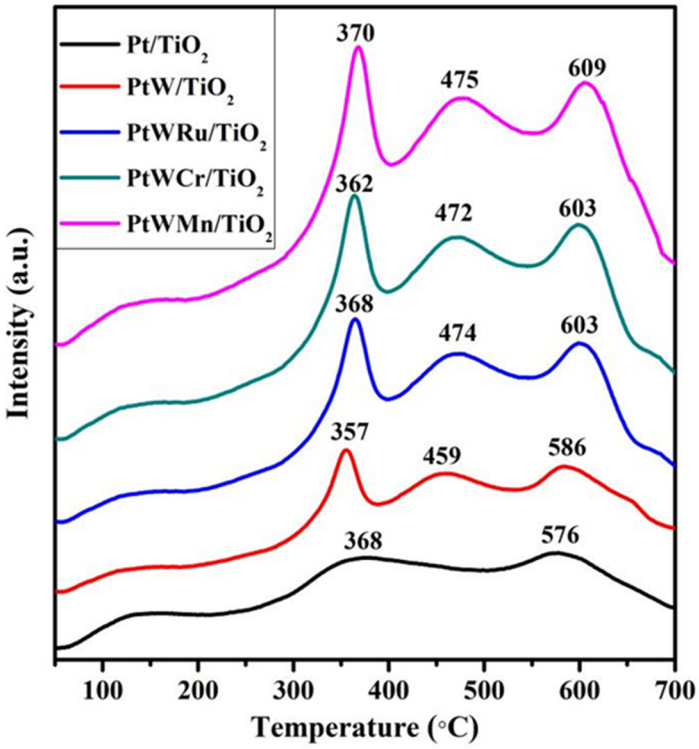

Figure 7. NH_3-TPD profiles of the as-obtained samples.

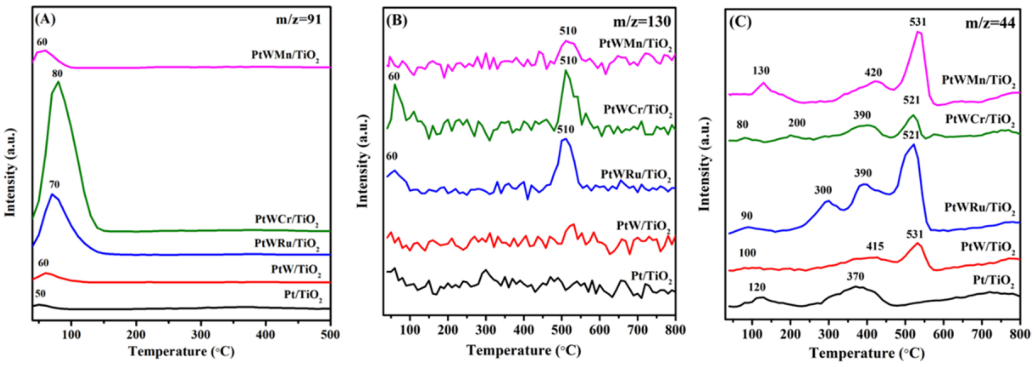

Figure 8. Toluene and TCE-TPD of the as-obtained samples: (**A**) m/z = 91 (toluene), (**B**) m/z = 130 (TCE), and (**C**) m/z = 44 (CO_2).

In addition, a mixed toluene and TCE temperature-programmed surface reaction (VOCs-TPSR) test was carried out, and the desorption species were analyzed by mass spectrometry (MS) to better assess each sample in the reaction process (as shown in Figure 9). For each sample, the desorption peaks of HCl were observed, as shown in Figure 9B. The primary temperature of HCl desorption emerged at about 200–250 °C on $PtWM/TiO_2$, while PtW/TiO_2 and Pt/TiO_2 were observed at about 300–400 °C. These results showed that chlorine desorption mainly occurred above these temperatures over the as-obtained catalysts. These results were attributed to PtW/TiO_2 and Pt/TiO_2, which were unavoidably deactivated as a result of chlorination at temperatures lower than 300–400 °C. Additionally, the amount of HCl that formed over the ternary metal catalyst was much higher than over PtW/TiO_2 and Pt/TiO_2, revealing that the increase in acidity promoted the formation of HCl, which was in line with the results of NH_3-TPD. Valid HCl desorption was also found to control the chlorination of the intermediate products, such as electrophilic chlorination [37]. Figure 9C shows the desorption signal of chlorobenzene (m/z = 112), which was one of the main products of toluene and TCE co-oxidation. The formation of more chlorobenzene on the Pt/TiO_2 catalyst was possibly attributed to insufficient acidity (elimination of Cl active

sites). Figure 9D shows the desorption signal of tetrachloroethylene (m/z = 166), which was one of the main products of TCE oxidation. For Pt/TiO_2, the formation of a variety of intermediates was possibly due to the lack of acid sites and reactive lattice oxygen species, which limited the complete catalytic oxidation of VOCs. The formation of these chlorine byproducts allowed them to react with each other and produced more toxic products such as dioxins, which can seriously harm the environment.

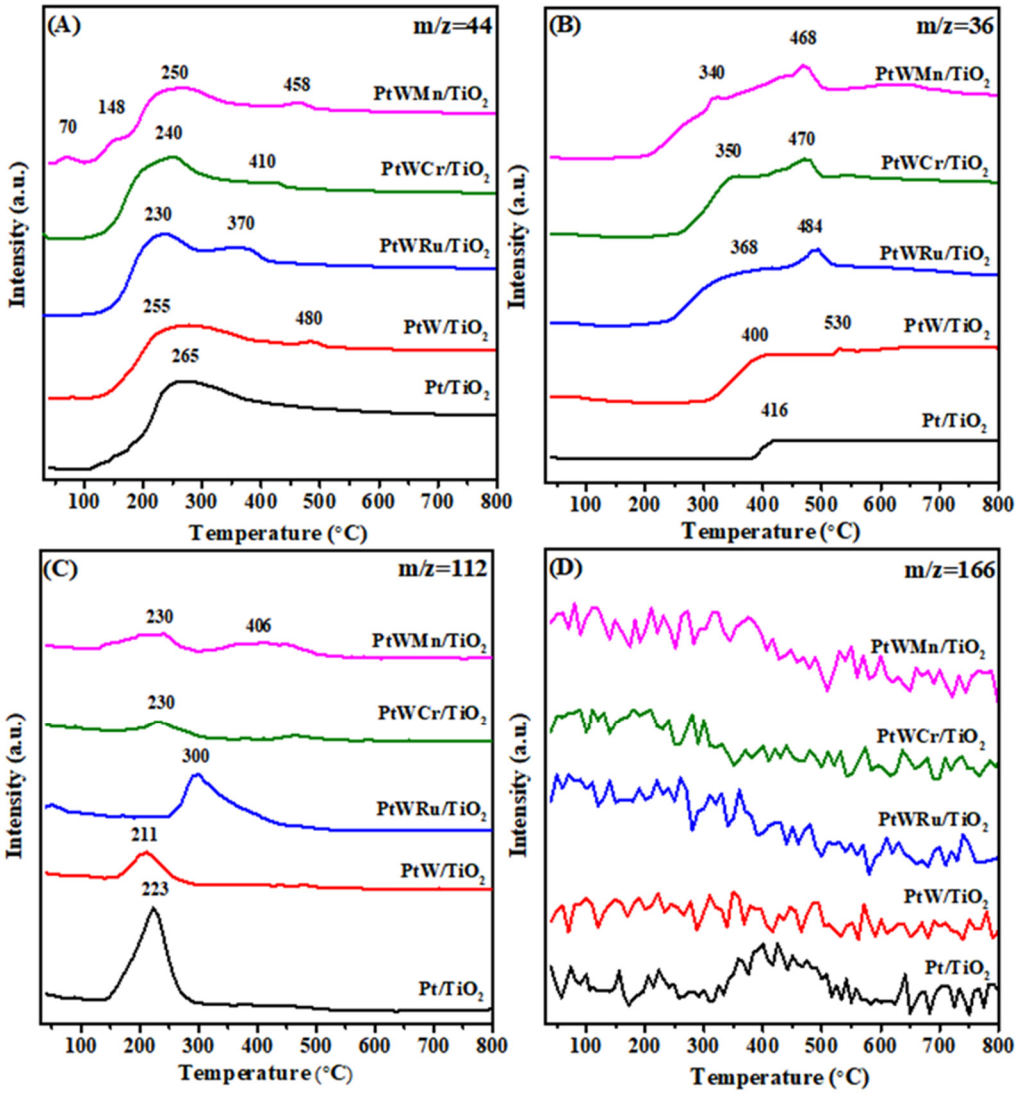

Figure 9. Toluene and TCE-TPSR of the as-obtained samples: (**A**) m/z = 44 (CO_2), (**B**) m/z = 36 (HCl), (**C**) m/z = 112 (C_6H_5Cl), and (**D**) m/z = 166 (C_2Cl_4).

2.6. GC-MS and In Situ DRIFTS

The reaction products were determined by TD-GC-MS, where the selected reaction temperature was 90% TCE conversion, at which time toluene underwent complete combustion. As shown in Figure 10, hydrogen chloride (HCl) and trichloroethanol (CCl_3CH_2OH) were the main intermediates over the supported ternary metal catalyst. Of note, other types of byproducts (chlorobenzene and benzene) were also detected, and no HCl or CCl_3CH_2OH species were detected over PtW/TiO_2 and Pt/TiO_2. These results indicated that the accumulation of chlorine species on the catalyst resulted in the production of chlorine-containing intermediates. For catalysts with good chlorine desorption, HCl and alcohol species were generated. The formation of the latter through H bonds between Ti–OH and Cl atoms allowed for trichloroethylene adsorption, following interaction with

M^{n+}=O (*M* = Ru, Cr, Mn) species on the surface of PtW, forming active enolic species, which could be further oxidized with surface oxygen species [36].

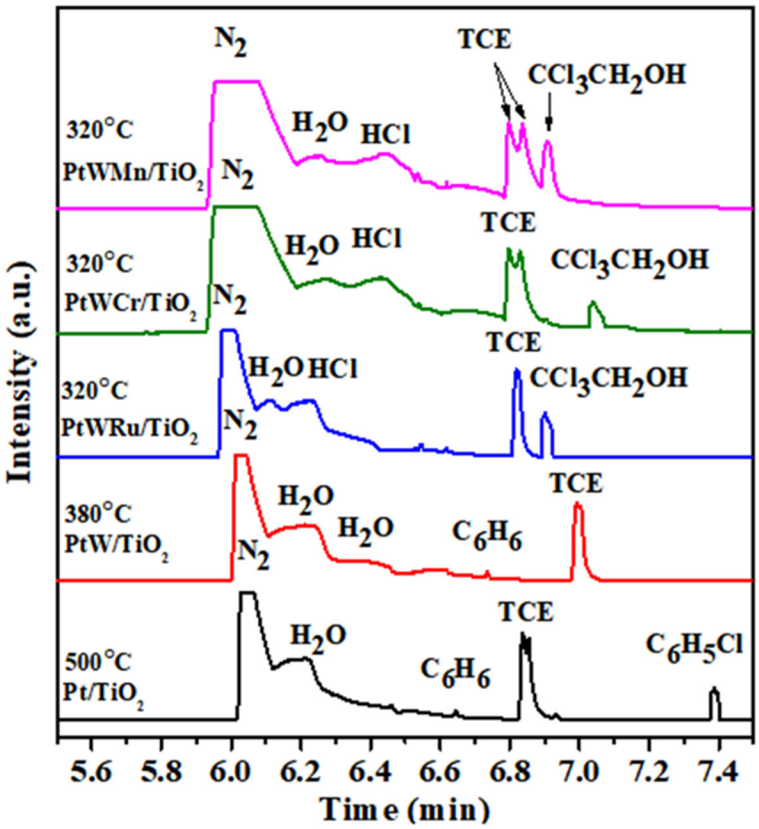

Figure 10. Possible reaction intermediates detected during mixed VOC oxidation over the as-obtained samples.

In situ DRIFTS characterization of the samples was conducted to explore the possible intermediate species from the reaction process and the reaction mechanism of toluene and TCE oxidation on the catalyst (as shown in Figure 11). The spectra acquired over the as-obtained catalysts for mixed VOC oxidation at 50–400 °C showed the involvement of toluene and TCE, as well as the intermediate products. The absorption peaks at 3853 cm^{-1}, 3750 cm^{-1}, and 3648 cm^{-1} were attributed to the vibrations of –OH [39]. The $–CH_2–$ absorption peak at 2930 cm^{-1} corresponded to the carbon–hydrogen stretching vibration, which belonged to the alkyl group of toluene [40]. In addition, 1602 cm^{-1} and 1456 cm^{-1} were attributed to the benzene ring vibration peaks of the toluene [41,42]. The absorption peaks at 1365 cm^{-1} and 1098 cm^{-1} consisted of the C–O bond stretching vibrations and alcoholic hydroxyl group bond in-plane bending vibrations [43,44]. Furthermore, 1699 cm^{-1} and 1684 cm^{-1} were the absorption peaks of the C=C bond [45]; as the temperature rises, the signal peaks of C=C become weaker on $PtWRu/TiO_2$ and also stronger on Pt/TiO_2, indicating that the TCE molecule is not completely oxidized on Pt/TiO_2 during the catalytic oxidation process. According to analysis with the mixed VOCs-TPSR, this was due to the byproducts. In addition, according to the catalytic activity test, TCE was difficult to completely oxidize, even at 500 °C on the catalysts. The characteristic peak at 1614 cm^{-1} was attributed to water [46], indicating that water did not form at low temperatures (<110 °C) over Pt/TiO_2. The details are listed in Supplementary Materials Table S2.

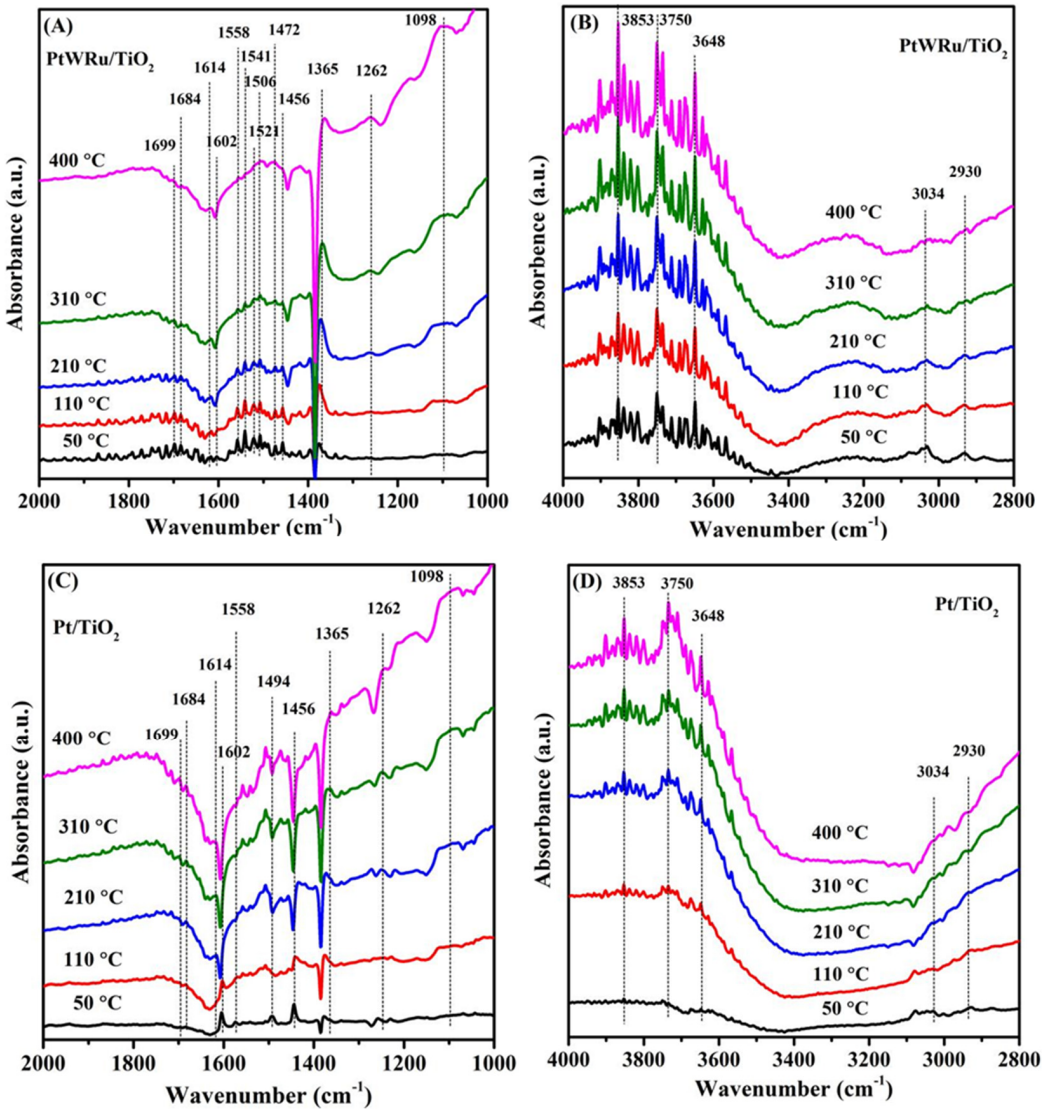

Figure 11. In situ DRIFTS spectra of (**A**,**B**) PtWRu/TiO_2 and (**C**,**D**) Pt/TiO_2 during VOC oxidation at different temperatures, where the reaction conditions were: 1000 ppm toluene + 200 ppm TCE + 20 vol% O_2 + N_2 (balanced), and SV = 40,000 mL/(g h).

3. Materials and Methods

3.1. Preparation of the Catalysts

Ternary metal nanoparticles (PtWRu) were first prepared according to a modified solvothermal method [17]. First, 5.11 mg of acetyl acetone platinum was weighed in 1-octadecene (2.5 mL), oleylamine (2.5 mL), and 0.5 mL oleic (0.5 mL) acid, which was mixed, stirred, and allowed to dissolve at room temperature for 20 min. *L*-ascorbic acid (49.32 mg) was added and stirred for 10 min. Then, 49.27 mg of $W(CO)_6$ and 21.31 mg of $Ru_3(CO)_{12}$ were added into the mixed solution, which was further stirred at room temperature for 20 min, and the acquired solution was shifted in a 10 mL sealed reaction vessel and reacted at 200 °C for 8 h. After cooling to room temperature, the reacted solution was centrifuged three to four times with the mixed cyclohexane and ethanol solution to obtain the PtWRu NPs. The prepared PtWRu NPs were uniformly dispersed into approximately 10 mL of cyclohexane for preservation. Then, the as-obtained PtWRu NPs were loaded onto a commercial TiO_2 carrier by the adsorption method, PtWRu/TiO_2 was further calcined at 300 °C for 2 h in a muffle furnace, and the PtWRu/TiO_2 catalyst was obtained (theoretical Pt loading = 0.5 wt%). The synthesis conditions of the PtWCr/TiO_2 and PtWMn/TiO_2

catalysts were similar to those of the PtWRu/TiO_2, catalyst, except for the use of $Cr(CO)_6$ (22.01 mg) and $Mn_2(CO)_{10}$ (22.01 mg).

The Pt NPs were also prepared according to the liquid-phase reduction method. First, 49.95 mg of acetyl acetone platinum, 10 mL of 1-octadecene, 1 mL of oleylamine, and 1 mL of oleic acid were added into a 3-necked flask and then stirred at room temperature until dissolved. The obtained mixed solution was then slowly heated to 120 °C under nitrogen gas and stirred at this temperature for another 0.5 h. Subsequently, the mixed solution was slowly heated (3–5 °C/min) to 200 °C, and the reaction was continued at this temperature for 0.5 h. The solution was centrifuged and washed with cyclohexane and ethanol three times, and then finally it was dispersed in cyclohexane (10 mL). The as-obtained Pt NPs were loaded onto the commercial TiO_2 carrier by the adsorption method, and Pt/TiO_2 was further calcined at 300 °C for 2 h in a muffle furnace.

The RuW/TiO_2 catalyst was prepared using the wet impregnation method. First, 20.7 mg of ruthenium chloride ($RuCl_3$) and 37.69 mg of ammonium metatungstate ($H_{28}N_6O_{41}W_{12}$) were dissolved in about 5 mL of deionized water at room temperature under continuous stirring, then 500 mg of commercial TiO_2 was added into the solution, followed by stirring continuously at room temperature and drying in an oven at 110 °C for 24 h. RuW/TiO_2 was further calcined at 500 °C for 2 h in a muffle furnace. The synthesis conditions of the CrW/TiO_2 and MnW/TiO_2 catalysts were similar to those of the RuW/TiO_2 catalyst, except for the use of $CrCl_3$ (26.65 mg) and $MnCl_2$ (19.8 mg).

3.2. Catalyst Characterization

The physicochemical properties of the as-obtained samples were measured using ICP-AES (Thermo Electron IRIS Intrepid ER/S spectrometer); XRD (Bruker/AXS D8 Advance diffractometer, with Cu Kα radiation and nickel filter (λ = 0.15406 nm)); BET (Micromeritics ASAP 2020 analyzer); TEM (JEOL JEM-2010 instrument); XPS (Thermo Fisher Scientific ESCALAB 250 Xi spectrometer) H_2-TPR (AutoChem II 2920, Micromeritics); O_2-TPD (AutoChem II 2920, Micromeritics); NH_3-TPD (AutoChem1 II 2920; BelCata II, Japan); (toluene and TCE)-TPD (AutoChem II 2920, Micromeritics); (toluene and TCE)-TPSR (AutoChem II 2920, Micromeritics); GC-MS (GC-2014C, Shimadzu) and in situ DRIFTS techniques (Nicolet 6700 FT-IR spectrometer with a liquid-nitrogen-cooled MCT detector). The detailed characterization procedures are provided in the supplementary materials section.

3.3. Catalytic Activity Evaluation

The catalytic activity of the as-obtained samples was determined in a fixed-bed quartz tubular microreactor (i.d. = 6.0 mm), where the samples (25 mg, 40–60 mesh) were mixed with quartz sand (125 mg, 40–60 mesh) to minimize the influence of hot spots. Before testing, the as-obtained samples were handled in the air (20 mL/min) at 250 °C for 1 h. The reaction mixture consisted of 1000 ppm toluene + 20 vol% O_2 + N_2 (balance), where 1000 ppm toluene was generated by passing N_2 flow through a pure toluene-containing bottle that was chilled in an isothermal bath at 10°C. The total flow of the reaction flow was 16.7 mL/min, giving a space velocity (SV) of 40,000 mL/(g·h). For trichloroethylene (TCE) addition, 200 ppm TCE was introduced from the cylinder with N_2 as the balance gas. The reaction gas mixture contained 1000 ppm toluene, 200 ppm TCE, 20 vol% O_2, and N_2 (balance), and the total flow of the reaction was 16.7 mL/min with SV = 40,000 mL/(g·h)). The reaction mixtures were analyzed using an online gas chromatograph (GC-7890). Toluene and TCE conversions (X%) were calculated by:

$$X = (c_{\text{inlet}} - c_{\text{outlet}})/c_{\text{inlet}} \times 100\% \quad (1)$$

where c_{inlet} and c_{outlet} denote the inlet and outlet toluene or TCE concentrations in the feed stream, respectively.

4. Conclusions

In this work, we synthesized ternary metal PtW*M* (*M* = Ru, Cr, Mn) NPs with uniform particle size distributions and subsequently prepared a series of PtW*M*/TiO_2 samples. In the oxidation of toluene, when TCE was added to the reaction system for 24 h, the conversion of toluene on Pt/TiO_2 and PtW/TiO_2 catalysts stabilized at 15% and 20%, respectively, and the conversion of toluene in PtWRu/TiO_2, PtWCr/TiO_2, and PtWMn/TiO_2 decreased to about 45.0%, 50.0%, and 45.0%, respectively. However, in the absence of TCE, toluene conversion could not restore over Pt/TiO_2 and PtW/TiO_2 catalysts within 12 h, while toluene conversion could be immediately recovered over PtWRu/TiO_2 and PtWCr/TiO_2. Among these samples, PtWRu/TiO_2 and PtWCr/TiO_2 showed the highest catalytic activity, the best toluene stability, and reversible trichloroethylene poisoning behavior. In the mixed VOC oxidation, the PtWCr/TiO_2 sample showed the best catalytic activity for toluene combustion (a toluene conversion of 90% was achieved at 258 °C and a space velocity of 40,000 mL g^{-1} h^{-1}, and the specific reaction rate and turnover frequency at 215 °C were 44.9×10^{-6} mol $g_{Pt}{}^{-1}$ s^{-1} and 26.2×10^{-5} s^{-1}). The PtWRu/TiO_2 sample showed the best catalytic activity for TCE combustion (a TCE conversion of 90% was achieved at 305 °C and a space velocity of 40,000 mL g^{-1} h^{-1}, and the specific reaction rate and turnover frequency at 270 °C were 9.0×10^{-6} mol $g_{Pt}{}^{-1}$ s^{-1} and 7.3×10^{-5} s^{-1}). According to the O_2-TPD results, PtW*M*/TiO_2 showed improvement in lattice oxygen mobility, which could promote the breakage of the C–Cl bond. In addition, there was an increase in Brønsted acidity in PtW*M*/TiO_2, which provides sufficient protons for HCl formation and inhibits the formation of Cl byproducts. This work provides a new strategy for the chlorine-resistant effects of supported Pt-based ternary metal catalysts for the simultaneous catalytic purification of VOCs and CVOCs.

Supplementary Materials: Supplementary data associated with this article can be found at https://www.mdpi.com/article/10.3390/catal12050541/s1, Figure S1: TEM images and particle size distributions of (a, A) Pt, (b, B) PtW, (c, C) PtWRu, (d, D) PtWCr, and (e, E) PtWMn NPs. Figure S2: (a) TEM and (b) HAADF-STEM images of Pt/TiO_2; (c) TEM and (d) HAADF-STEM images of PtW/TiO_2. Figure S3: (A) Nitrogen adsorption–desorption isotherms and (B) pore-size distributions of (a) Pt/TiO_2, (b) PtW/TiO_2, (c) PtWRu/TiO_2, (d) PtWCr/TiO_2, and (e) PtWMn/TiO_2. Table S1: $T_{50\%}$ and $T_{90\%}$ on the as-obtained samples. Figure S4: Toluene conversion as a function of temperature over the samples (solid curves: in the absence of TCE; dotted curves: in the presence of 200 ppm TCE). Figure S5: XPS spectra of (A) Pt 4f, (B) Ti 2p, and (C) W 4f in each sample. Table S2: Assignments of the DRIFTS bands of the samples.

Author Contributions: Conceptualization, H.D. and Y.L.; Methodology, T.D.; Software, T.D. and H.C.; Investigation, R.G.; Resources, Y.L.; Data Curation, T.D., X.Y. and Z.H.; Writing—Original Draft Preparation, T.D.; Writing—Review and Editing, T.D.; Visualization, K.L.; Supervision, K.L., L.J. and J.D.; Project Administration, Y.L.; Funding Acquisition, Y.L. All authors have read and agreed to the published version of the manuscript.

Funding: This work was supported by the National Natural Science Foundation of China, grant number 21976009 and 21876006; National Natural Science Committee of China—Liaoning Provincial People's Government Joint Fund, grant number U1908204; Foundation on the Creative Research Team Construction Promotion Project of Beijing Municipal Institutions, grant number IDHT20190503; Development Program for the Youth Outstanding—Notch Talent of Beijing Municipal Commission of Education, grant number CIT&TCD201904019.

Data Availability Statement: All the relevant data used in this study have been provided in the form of figures and tables in the published article, and all data provided in the present manuscript are available to whom it may concern.

Conflicts of Interest: The authors declare no conflict of interest.

References

1. Kim, J.M.; Lee, C.Y.; Jerng, D.W.; Ahn, H.S. Toluene and acetaldehyde removal from air on to graphene-based adsorbents with microsized pores. *J. Hazard. Mater.* **2018**, *344*, 458–465. [CrossRef] [PubMed]
2. Li, W.B.; Wang, J.X.; Gong, H. Catalytic conbustion of VOCs on non-noble metal catalyst. *Catal. Today* **2009**, *148*, 81–87. [CrossRef]
3. Lu, C.-Y.; Wey, M.-Y. Simultaneous removal of VOC and NO by activated carbon impregnated with transition metal catalysts in combustion flue gas. *Fuel Process. Technol.* **2007**, *88*, 557–567. [CrossRef]
4. Drago, R.S.; Jurczyk, K.; Singh, D.J.; Young, V. Low-temperature deep oxidation of hydrocarbons by metal oxides supported on carbonaceous materials. *Appl. Catal. B Environ.* **1995**, *6*, 155–168. [CrossRef]
5. Sun, P.F.; Wang, W.L.; Weng, X.L.; Dai, X.X.; Wu, Z.B. Alkali Potassium Induced HCl/CO_2 selectivity enhancement and chlorination reaction inhibition for catalytic oxidation of chloroaromatics. *Environ. Sci. Technol.* **2018**, *52*, 6438–6447. [CrossRef] [PubMed]
6. Zhang, X.; Dai, L.; Liu, Y.; Deng, J.; Jing, L.; Yu, X.; Han, Z.; Zhang, K.; Dai, H. 3DOM CeO_2-supported Ru_yM (M = Au, Pd, Pt) alloy nanoparticles with improved catalytic activity and chlorine-tolerance in trichloroethylene oxidation. *Catal. Sci. Technol.* **2020**, *10*, 3755–3770. [CrossRef]
7. Yang, P.; Fan, S.; Chen, Z.; Bao, G.; Zuo, S.; Qi, C. Synthesis of Nb_2O_5 based solid superacid materials for catalytic combustion of chlorinated VOCs. *Appl. Catal. B Environ.* **2018**, *239*, 114–124. [CrossRef]
8. Weon, S.; Kim, J.; Choi, W. Dual-components modified TiO_2 with Pt and fluoride as deactivation-resistant photocatalyst for the degradation of volatile organic compound. *Appl. Catal. B Environ.* **2018**, *220*, 1–8. [CrossRef]
9. Avgouropoulos, G.; Oikonomopoulos, E.; Kanistras, D.; Ioannides, T. Complete oxidation of ethanol over alkali-promoted Pt/Al_2O_3 catalysts. *Appl. Catal. B Environ.* **2006**, *65*, 62–69. [CrossRef]
10. Hosseini, M.; Siffert, S.; Cousin, R.; Aboukaïs, A.; Hadj-Sadok, Z.; Su, B.L. Total oxidation of VOCs on Pd and/or Au supported on TiO_2/ZrO_2 followed by "operando" DRIFT. *C. R. Chim.* **2009**, *12*, 654–659. [CrossRef]
11. Chen, G.; Zhao, Y.; Fu, G.; Duchesne, P.N.; Gu, L.; Zheng, Y.; Weng, X.; Chen, M.; Zhang, P.; Pao, C.-W.; et al. Interfacial Effects in Iron-Nickel Hydroxide–Platinum Nanoparticles Enhance Catalytic Oxidation. *Science* **2014**, *344*, 495–499. [CrossRef] [PubMed]
12. Priya, M.; Kiruthika, S.; Muthukumaran, B. Synthesis and characterization of Pt-Sn-Ce/MC ternary catalysts for ethanol oxi-dation in membraneless fuel cells. *Ionics* **2017**, *23*, 1209–1218. [CrossRef]
13. Yang, J.; Liu, Y.X.; Deng, J.G.; Zhao, X.T.; Zhang, K.F.; Han, Z.; Dai, H.X. AgAuPd/meso-Co_3O_4: High-performance catalysts for methanol oxidation. *Chin. J. Catal.* **2019**, *40*, 837–848. [CrossRef]
14. García, T.; Solsona, B.; Taylor, S.H. The Oxidative Destruction of Hydrocarbon Volatile Organic Compounds Using Palladium–Vanadia–Titania Catalysts. *Catal. Lett.* **2004**, *97*, 99–103. [CrossRef]
15. Huang, H.B.; Leung, D.Y.C. Complete oxidation of formaldehyde at room temperature using TiO_2 supported metallic Pd na-noparticles. *ACS Catal.* **2011**, *1*, 348–354. [CrossRef]
16. Brink, R.V.D.; Krzan, M.; Feijen-Jeurissen, M.; Louw, R.; Mulder, P. The role of the support and dispersion in the catalytic combustion of chlorobenzene on noble metal based catalysts. *Appl. Catal. B Environ.* **2000**, *24*, 255–264. [CrossRef]
17. Zhang, K.Y.; Dai, L.Y.; Liu, Y.X.; Deng, J.G.; Jing, L.; Zhang, K.F.; Hou, Z.Q.; Zhang, X.; Wang, J.; Feng, Y.; et al. Insights into the active sites of chlorine-resistant Pt-basedbimetallic catalysts for the oxidative removal of benzene. *Appl. Catal. B* **2020**, *279*, 119372. [CrossRef]
18. Dai, Q.; Wang, W.; Wang, X.; Lu, G. Sandwich-structured CeO_2@ZSM-5 hybrid composites for catalytic oxidation of 1, 2-dichloroethane: An integrated solution to coking and chlorine poisoning deactivation. *Appl. Catal. B Environ.* **2017**, *203*, 31–42. [CrossRef]
19. Zhang, Z.; Huang, J.; Xia, H.Q.; Dai, Q.G.; Gu, Y.F.; Lao, Y.J.; Wang, X.Y. Chlorinated volatile organic compound oxidation over SO_4^{2-}/Fe_2O_3 catalysts. *J. Catal.* **2018**, *360*, 277–289. [CrossRef]
20. Weng, X.; Meng, Q.; Liu, J.; Jiang, W.; Pattisson, S.; Wu, Z. Catalytic Oxidation of Chlorinated Organics over Lanthanide Perovskites: Effects of Phosphoric Acid Etching and Water Vapor on Chlorine Desorption Behavior. *Environ. Sci. Technol.* **2018**, *53*, 884–893. [CrossRef]
21. Fang, C.; Jiang, X.; Hu, J.; Song, J.; Sun, N.; Zhang, D.; Kuai, L. Ru Nanoworms Loaded TiO_2 for Their Catalytic Performances toward CO Oxidation. *ACS Appl. Mater. Interfaces* **2021**, *13*, 5079–5087. [CrossRef] [PubMed]
22. Hu, J.; Wang, F.; Li, Y.; Lv, H.; Sun, M.; Zhai, Y.; Lv, G.; Zhang, X. Enhanced catalytic performance of oxidized Ru supported on N-doped mesoporous carbon for acetylene hydrochlorination. *Appl. Catal. A Gen.* **2021**, *623*, 118236. [CrossRef]
23. Liang, Y.; Liu, Y.; Deng, J.; Zhang, K.; Hou, Z.; Zhao, X.; Zhang, X.; Zhang, K.; Wei, R.; Dai, H. Coupled Palladium–Tungsten Bimetallic Nanosheets/TiO_2 Hybrids with Enhanced Catalytic Activity and Stability for the Oxidative Removal of Benzene. *Environ. Sci. Technol.* **2019**, *53*, 5926–5935. [CrossRef] [PubMed]
24. Xiao, Q.; Wang, Y.; Zhao, Z.-J.; Pei, C.; Chen, S.; Gao, L.; Mu, R.; Fu, Q.; Gong, J. Defect-mediated reactivity of Pt/TiO_2 catalysts: The different role of titanium and oxygen vacancies. *Sci. China Ser. B Chem.* **2020**, *63*, 1323–1330. [CrossRef]
25. Zhang, W.; Shi, X.; Shan, Y.; Liu, J.; Xu, G.; Du, J.; Yan, Z.; Yu, Y.; He, H. Promotion effect of cerium doping on iron–titanium composite oxide catalysts for selective catalytic reduction of NO_x with NH_3. *Catal. Sci. Technol.* **2020**, *10*, 648–657. [CrossRef]
26. Ettireddy, P.R.; Ettireddy, N.; Mamedov, S.; Boolchand, P.; Smirniotis, P.G. Surface characterization studies of TiO_2 supported manganese oxide catalysts for low temperature SCR of NO with NH_3. *Appl. Catal. B Environ.* **2007**, *76*, 123–134. [CrossRef]

27. Sun, M.M.; Liu, J.Y.; Song, C.; Ogata, Y.; Rao, H.B.; Zhao, X.Q.; Xu, H.D.; Chen, Y.Q. Different reaction mechanisms of am-monia oxidation reaction on Pt/Al_2O_3 and $Pt/CeZrO_2$ with various Pt states. *ACS Appl. Mater. Interfaces* **2019**, *11*, 23102–23111. [CrossRef]
28. Chen, Y.; Huang, Z.; Zhou, M.; Ma, Z.; Chen, J.; Tang, X. Single Silver Adatoms on Nanostructured Manganese Oxide Surfaces: Boosting Oxygen Activation for Benzene Abatement. *Environ. Sci. Technol.* **2017**, *51*, 2304–2311. [CrossRef]
29. Yang, Y.; Li, H.; Zhao, H.; Qu, R.; Zhang, S.; Hu, W.; Yu, X.; Zhu, X.; Liu, S.; Zheng, C.; et al. Structure and crystal phase transition effect of Sn doping on anatase TiO_2 for dichloromethane decomposition. *J. Hazard. Mater.* **2019**, *371*, 156–164. [CrossRef]
30. Miao, S.; Liu, Z.; Han, B.; Huang, J.; Sun, Z.; Zhang, J.; Jiang, T. Ru Nanoparticles Immobilized on Montmorillonite by Ionic Liquids: A Highly Efficient Heterogeneous Catalyst for the Hydrogenation of Benzene. *Angew. Chem. Int. Ed.* **2006**, *45*, 266–269. [CrossRef]
31. Zeng, L.; Wan, B.; Huang, R.; Yan, Y.; Wang, X.; Tan, W.; Liu, F.; Feng, X. Catalytic oxidation of arsenite and reaction pathways on the surface of CuO nanoparticles at a wide range of pHs. *Geochem. Trans.* **2018**, *19*, 12. [CrossRef] [PubMed]
32. Lin, F.W.; Wang, Z.; Zhang, Z.M.; Xiang, L.; Yuan, D.K.; Yan, B.B.; Wang, Z.H.; Chen, G.Y. Comparative investigation on chlorobenzene oxidation by oxygen and ozone over a MnO_x/Al_2O_3 catalyst in the presence of SO_2. *Environ. Sci. Technol.* **2021**, *55*, 3341–3351. [CrossRef] [PubMed]
33. Yang, L.; Ma, J.Z.; Li, X.T.; Zhang, C.B.; He, H. Enhancing oxygen vacancies of Ce-OMS-2 via optimized hydrothermal con-ditions to improve catalytic ozone decomposition. *Ind. Eng. Chem. Res.* **2019**, *59*, 118–128. [CrossRef]
34. Dai, Q.; Zhu, Q.; Lou, Y.; Wang, X. Role of Brønsted acid site during catalytic combustion of methane over PdO/ZSM-5: Dominant or negligible? *J. Catal.* **2018**, *357*, 29–40. [CrossRef]
35. Ardagh, M.A.; Bo, Z.; Nauert, S.L.; Notestein, J.M. Depositing SiO_2 on Al_2O_3: A Route to Tunable Brønsted Acid Catalysts. *ACS Catal.* **2016**, *6*, 6156–6164. [CrossRef]
36. Sun, W.; Gong, B.W.; Pan, J.; Wang, Y.Y.; Xia, H.Q.; Zhang, H. Catalytic combustion of CVOCs over Cr_xTi_{1-x} oxide catalysts. *J. Catal.* **2020**, *391*, 132–144. [CrossRef]
37. Gu, Y.; Jiang, X.; Sun, W.; Bai, S.; Dai, Q.; Wang, X. 1,2-Dichloroethane Deep Oxidation over Bifunctional Ru/Ce_xAl_y Catalysts. *ACS Omega* **2018**, *3*, 8460–8470. [CrossRef]
38. Iwasaki, M.; Iglesia, E. Mechanistic assessments of NO oxidation turnover rates and active site densities on WO_3-promoted CeO_2 catalysts. *J. Catal.* **2016**, *342*, 84–97. [CrossRef]
39. Hetrick, C.E.; Lichtenberger, J.; Amiridis, M.D. Catalytic oxidation of chlorophenol over V_2O_5/TiO_2 Catalysts. *Appl. Catal. B* **2008**, *77*, 255–263. [CrossRef]
40. Chen, J.; Xu, W.; Jiang, M.; Jia, H. Polyoxometallate functionalizing CeO_2 via redox-etching precipitation to synergistically catalyze oxidation of gaseous chlorinated pollutants: From lab to practice. *Appl. Catal. B Environ.* **2020**, *278*, 119263. [CrossRef]
41. Liao, Y.; Zhang, X.; Peng, R.; Zhao, M.; Ye, D. Catalytic properties of manganese oxide polyhedra with hollow and solid morphologies in toluene removal. *Appl. Surf. Sci.* **2017**, *405*, 20–28. [CrossRef]
42. Besselmann, S.; Löffler, E.; Muhler, M. On the role of monomeric vanadyl species in toluene adsorption and oxidation on V_2O_5/TiO_2 catalysts: A Raman and in situ DRIFTS study. *J. Mol. Catal. A* **2000**, *162*, 401–411. [CrossRef]
43. Rainone, F.; Bulushev, D.A.; Kiwi-Minsker, L.; Renken, A. DRIFTS and transient-response study of vanadia/titania catalysts during toluene partial oxidation. *Phys. Chem. Chem. Phys.* **2003**, *5*, 4445–4449. [CrossRef]
44. Li, J.; Na, H.; Zeng, X.; Zhu, T.; Liu, Z. In situ DRIFTS investigation for the oxidation of toluene by ozone over Mn/HZSM-5, Ag/HZSM-5 and Mn–Ag/HZSM-5 catalysts. *Appl. Surf. Sci.* **2014**, *311*, 690–696. [CrossRef]
45. Wu, W.-C.; Liao, L.-F.; Lien, C.-F.; Lin, J.-L. FTIR study of adsorption, thermal reactions and photochemistry of benzene on powdered TiO_2. *Phys. Chem. Chem. Phys.* **2001**, *3*, 4456–4461. [CrossRef]
46. Fu, X.H.; Liu, Y.X.; Deng, J.G.; Jing, L.; Zhang, X.; Zhang, K.F.; Han, Z.; Jiang, X.Y.; Dai, H.X. Intermetallic compound PtMny-derived Pt-MnO_x supported on mesoporous CeO_2: Highly efficient catalysts for the combustion of toluene. *Appl. Catal. A* **2020**, *595*, 117509. [CrossRef]